Water Supply

IWA PUBLISHING

Water Supply Vol 22 No 5, 4798 doi: 10.2166/ws.2022.141

Composite membrane of polyguanidine cationic surface for desalination

Qingfeng Han[a], Dongqing Liu[b,*], Xiaohua Huang[a], Qinxing Xie[b] and Jianqiang Meng[b]

[a] Tiangong University, No.399 BinShuiXi Road, XiQing District, Tianjin, China
[b] State Key Laboratory of Separation Membranes and Membrane Processes, Tianjin Key Laboratory of Hollow Fiber Membrane Materials and Processes, School of Material Science and Engineering, Tiangong University, Tianjin 300387, China
*Corresponding author. E-mail: ldqnov@163.com

DL, 0000-0002-3621-6319

ABSTRACT

Surface positve-charged composite membranes were prepared through two guanidine group containing polymers, polyhexamethylene guanidine (PHMG) and polyhexamethylene biguanidine (PHMB). They were used as aqueous phase monomers in an interfacial polymerization (IP) process reacting with trimesoyl chloride (TMC) on the surface of polysulfone (Psf) ultrafiltration membrane. Piperazine (PIP) provided the best pH adjustment among the chosen regulators. As guanidine groups dissociate in water and bring ammonium cations to membrane surfaces, both polyguanidine endowed membranes reacted with divalent metal cations better compared with Na^+ and Li^+. The rejection rates were more than 90% for all chosen divalent metal salts. PHMG membranes displayed excellent enrichment of Li^+ from a mixed solution of Mg^{2+} and Li^+ salts. The Mg^{2+}/Li^+ mass ratio decreased from 60 to 3.7, accompanying a −3.6% rejection to Li^+. Although partial guanidine groups participated in the IP reaction, bactericidal rates of membranes were both higher than 99% in Gram-negative *E. coli* and Gram-positive *S. aureus* tests.

Key words: antibacteria, cationic-charged membrane, heavy metal cation removal, lithium enrichment, polyguanidine

HIGHLIGHTS

- Removal of harmful heavy metal ions.
- Multiple metal ion removal.
- Excellent separation of magnesium and lithium.
- Nanofiltration membrane against microbial contamination.
- Cation surface nanofiltration membrane.

GRAPHICAL ABSTRACT

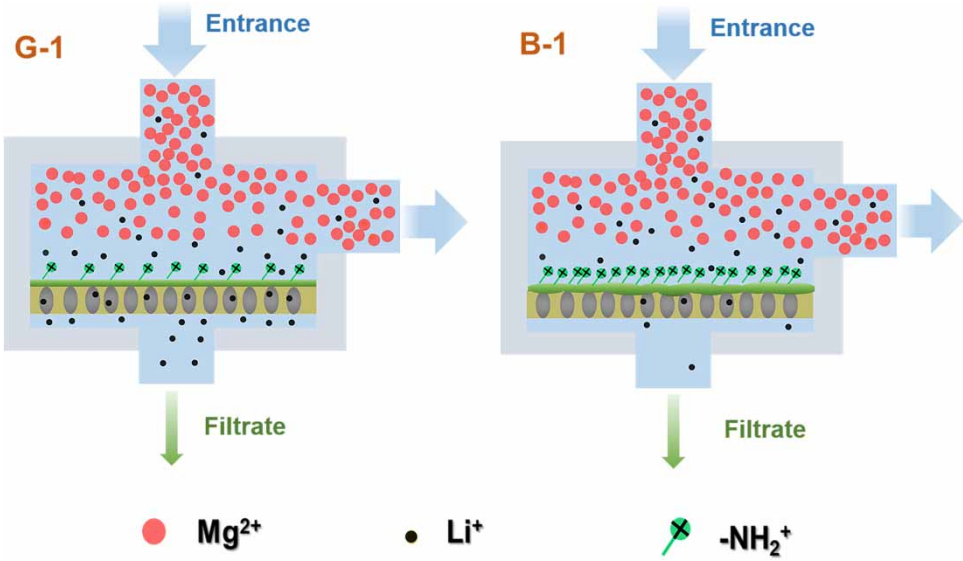

1. INTRODUCTION

As global temperatures increase, environment deterioration and the energy crisis become more and more serious (Bodzek *et al.* 2020). Pollution control and resource utilization are imperative in various fields including water, soil and air on the Earth (Ahmad *et al.* 2021). In water treatment areas, separation membrane techniques have displayed special advantages in contaminant treatment and resource collection and enrichment owing to the merits of energy saving, simple operation and moderate space occupation. Among numerous membrane techniques, the nanofiltration (NF) membrane has an important place in soluble separation and hazardous substance removal (Domenech *et al.* 2020). NF techniques could achieve accurate particle size screening under pore size sieve mechanisms and the Donnan effect (Mohammad *et al.* 2015; Bi *et al.* 2020). It has displayed great potential in many fields, including sea water desalination (Padaki *et al.* 2011), toxic heavy metal ion and dye removal (Qi *et al.* 2019) and separation of $Li^+/Mg^{2+}$from their nature mixed solution, such as some salt lakes (Sun *et al.* 2021).

Among NF films, surface-charged membranes have attracted more and more attention due to excellent ion separation according to their sizes and chemical valence (Akbari *et al.* 2016; Fang *et al.* 2018). Particularly, positve-charged membrane produce more electric repulsion to multivalent cations than monovalent ones, which provides an outstanding removal efficiency for multivalence metal ions. Thin layer composite membrane techniques through interfacial polymerization (IP) is a convenient and popular method to prepare positve-charged NF membranes (Wang *et al.* 2011). Xu *et al.* (2019) prepared a positve charged composite membrane between polyethyleneimine (PEI) and TMC on a polyethersulfone (PES) ultrafiltration membrane. The membrane displayed great separation capacity for Mg^{2+} and Li^+. After filtration by the membrane, the Mg^{2+}/Li^+ mass ratio in mixed solution declined from an initial 20 to 1.3. The rejection for Mg^{2+} and Li^+ was high, up to 76%. Bi *et al.* (2021) functionalized nanographitic carbon nitride (g-C_3N_4) and used it as a monomer in the aqueous phase. The as-product positve-charged membrane effectively decreased the Mg^{2+}/Li^+ ratio from 73 to 1.85. In addition, the membrane showed excellent antifouling performance.

Commonly, compounds containing amine or sulfhydryl group could introduce positive charges to chemical structures through dissociation to ammonium or sulfonium cations. Polyguanidines, a series of oligomers full of NH groups in a backbone, also exhibited the potential to introduced positive charges to membrane surfaces. Li *et al.* (2014a) synthesized polyhexamethylene guanidine (PHMG) and used it as aqueous monomer under the pH regulation by triethylamine. The composite membrane of the cationic surface provided salt rejection in the order of $MgCl_2 > MgSO_4 > Na_2SO_4 > NaCl$. The highest rejection was 86.2% for $MgCl_2$. The membrane also exhibited wonderful antibacteria and antifouling capacity as PHMG was a polycation biocide (Chindera *et al.* 2016; Wang *et al.* 2020). Here, two polyguanidine were investigated as aqueous monomers to prepare an NF composite membrane with TMC *n*-hexane solution, including PHMG and polyhexamethylene biguanidine (PHMB). Piperazine (PIP) and other bases were investigated as pH regulators to adjust the functional layer structure. Guanidine-PIP

films were confirmed as positive-charged membranes, and showed high removal rates for metal cations, especially multivalent cations, such as Mg^{2+}, Pd^{2+} and Cd^{2+}. The PHMG membrane, G-1, could also enrich Li^{+} from the mixed solution of Mg^{2+} and Li^{+}. The membranes also exhibited excellent antibacterial ability towards *Escherichia coli* (E.C.) and *Staphylococcus aureus* (S.A.). Polyguanidines possessed attractive potential in the preparation of multifunctional membranes in water treatment.

2. EXPERIMENTAL

2.1. Materials

Polysulfone (Mw = 70,000, industrial purity) was supplied by Solvay Advanced Polymer (Belgium). PHMG and PHMB (M_W around 5,000) were kindly provided by Hebei Jinhong Chemical Co., Ltd. Trimesoyl chloride (TMC), tris(hydroxymethyl)aminomethane (Tris), and triethylamine (TEA) were purchased from Beijing J&K Scientific Co., Ltd. $MgCl_2$, $MgSO_4$, $NaSO_4$, NaCl, $Pb(NO_3)_2$, $Cd(NO_3)_2$ and LiCl came from Shanghai Titan Technology Co., Ltd. PSF ultrafiltration supporting membrane was prepared through Yu *et al.* (2009)'s method.

2.2. Preparation of polyguanidine composite membranes

PIP powder was slowly added into 3 wt% PHMB solution to adjust the pH. Then the aqueous solution was poured onto the PSF supporting membrane. After 30 min, the aqueous solution was poured out. A TMC solution (0.2 wt%) of *n*-hexane was added onto the membrane and discarded after 15 min (An *et al.* 2011). After full volatilization of residual *n*-hexane, the membranes were stored in deionized (DI) water. As a control, a 3 wt% PHMB aqueous solution was directly used as an aqueous monomer. The operations were all conducted at room temperature.

In base screening experiments, different bases were added into 3 wt% PHMB solution to adjust the pH. IP operation was the same as described above.

For the PHMG composite membrane, the operation was the same as above.

2.3. Characterization of membranes

Conductivity and pH of the solution were separately measured using a conductivity meter (FE38-Meter) and a pH meter (FE28-Standard) from Mettler-Toledo Instruments Ltd. The thickness of the PSF membrane was measured using a helical micrometer, and the pore size of PSF was measured using an automatic mercury porosimeter (AutoPore IV 9500, USA). The porosity was calculated using the following equation: $\varepsilon\ (\%) = 100 \times (1 - \rho_{Hg}/\rho_{He})$, where ε refers to the porosity, ρ_{Hg} and ρ_{He} refer to the density of mercury and helium. The concentrations of Mg^{2+} and Li^{+} were determined by ICP-OES (PerkinElmer 8300). Surface chemistry of the composite membrane was analyzed by attenuated total reflectance infrared (ATR-IR) spectroscopy by Nicolet IS50 infrared spectrometer (Thermo Fisher, USA). X-ray photoelectron spectrometry (XPS) analyses was graphed through a Thermo Fisher K-alpha spectrometer using focused monochromatized Al Kα radiation. An S-4800 field emission scanning electron microscope (FE-SEM, Hitachi, Japan) was used to observe surface and cross-section morphology of the membranes. The samples were sprayed with gold powder before testing. Average roughness (Ra) of the membrane surface was analyzed by atomic force microscopy (AFM, Bruker, Icon, USA) in a tapping mode. Dynamic water contact angle (DWCA) of the membrane surface was measured using a Drop Shape Analysis 100 contact angle meter (Kruss BmbH Co., Germany). Membrane surface charge properties were characterized by streaming zeta potential measurement containing a SurPASS electrokinetic analyzer (Anton Paar, Austria) at pH 2–10. Measurements were carried out with a 0.01 mol·L^{-1} KCl solution as the feed at 25 ± 1.0 °C; 0.01 mol·L^{-1} hydrochloric acid and sodium hydroxide solutions were used to adjust the pH of the solution.

2.4. Operation performance of membranes

Pure water flux (PWF) and filtration performance of membranes were evaluated using a home-made cross-flow device at room temperature under 0.5 MPa. The membrane was prepressed for 30 min before recording. All solution concentrations were fixed at 1.0 g·L^{-1}. The effluent was collected and analyzed for 30 minutes. The concentrations of feed solution and permeate were measured using a conductivity meter. Water flux of the salt solution (SWF), solute rejection rate (Li *et al.* 2019) and water flux recovery rate (FRR) (Meng *et al.* 2021) in membrane filtration operation were calculated using Equations (1)–(3), respectively:

$$J = \frac{V}{A \times \Delta t} \tag{1}$$

$$R = \left(1 - \frac{C_p}{C_f}\right) \times 100\% \tag{2}$$

$$FRR = \left(\frac{J_{W2}}{J_{W1}}\right) \times 100\% \tag{3}$$

where, V is effluent volume, A is effective membrane area, and Δt represents filtrate time from recording. C_p is the original solution concentration and C_f is the effluent concentration. J_{w1} is the initial flux and J_{w2} represents the initial flux of the next cycle.

2.5. Separation of Li^+ and Mg^{2+}

The concentration of $MgCl_2$ and LiCl mixed solution was 4 g·L^{-1} with the mass ratio of Mg^{2+}/Li^+ as 60. Metal cation contents in the effluent were measured by ICP-OES/MS. The rejection rates of Mg^{2+} and Li^+ were calculated according to Equation (2). The separation factor (Li *et al.* 2021) $S_{Li,Mg}$ was defined by Equation (4):

$$S_{Li,Mg} = \frac{C_{1,Mg}/C_{1,Li}}{C_{2,Mg}/C_{2,Li}} \tag{4}$$

where, $C_{1,Mg}$ and $C_{2,Mg}$ refer to the concentrations of Mg^{2+} in the feed and permeate, respectively. Similarly, $C_{1,Li}$ and $C_{2,Li}$ represent concentrations of Li^+ in the feed and permeate, separately.

2.6. Antibacteria tests

Antibacterial properties of the membranes were evaluated by shake flask tests using *E. coli* (E.C.) as the model Gram-negative bacteria and *S. aureus* (S.A.) as the Gram-positive model (Hou *et al.* 2009). The area of tested membrane was 5×10^{-4} m^2. The tests were operated according to the literature (Meng *et al.* 2015).

3. RESULTS AND DISCUSSION

The home-made base membrane was measured first. Its thickness was 140 μm and the average pore size was 120.2 nm with 56.10% porosity, see supplementary figure (Fig. S1).

3.1. Aqueous phase formulation optimization

Figure 1 shows the chemical structures of PHMG and PHMB, which were oligomeric products of hexanediamine with ammonia and sodium dicyanamide, respectively. They were polycations with an average of 12–16 biguanide groups spaced by hexamethylene segments. Solution pH of 3 wt% PHMG and PHMB were 8.9 and 7.7, respectively. Both of them could not provide satisfying rejection of $MgCl_2$, when they were used as aqueous monomers alone in the NF composite membranes preparation (Figure 2(a)). A 3 wt% PHMB solution was firstly chosen to optimize the aqueous phase formulation and then the PHMG membrane was prepared according to the optimized PHMB recipe. Pure PHMB solution prepared a membrane for 21.0% $MgCl_2$ rejection as the reactivity of its hydrochloride was very low; at pH values far lower than 11.8, compared with the value of the 3 wt% PIP solution. Five alkalines were investigated as pH regulators of aqueous phase. Overall, the rejection of membranes made from organic base displayed better performance than those from inorganic ones. NaOH and ammonium hydroxide provided very poor adjustment. PIP gave the best assistance because it not only regulated pH but also participated in the IP reaction to build compact cross-linking network. As PIP was added (Figure 2(b)), the rejection to $MgCl_2$ increased. At pH up to 11, $MgCl_2$ removal rate arrived at the apex, 99.6%. The mass ratio of PHMB to PIP was 6:1 at this point. As PIP

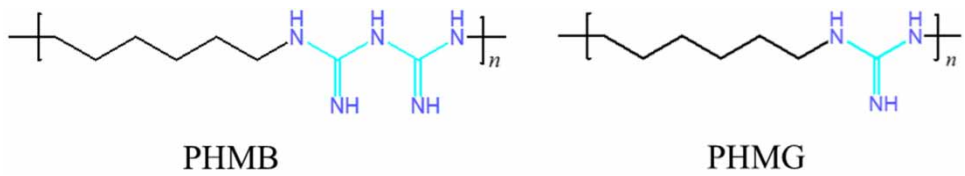

Figure 1 | Chemical structures of PHMB and PHMG.

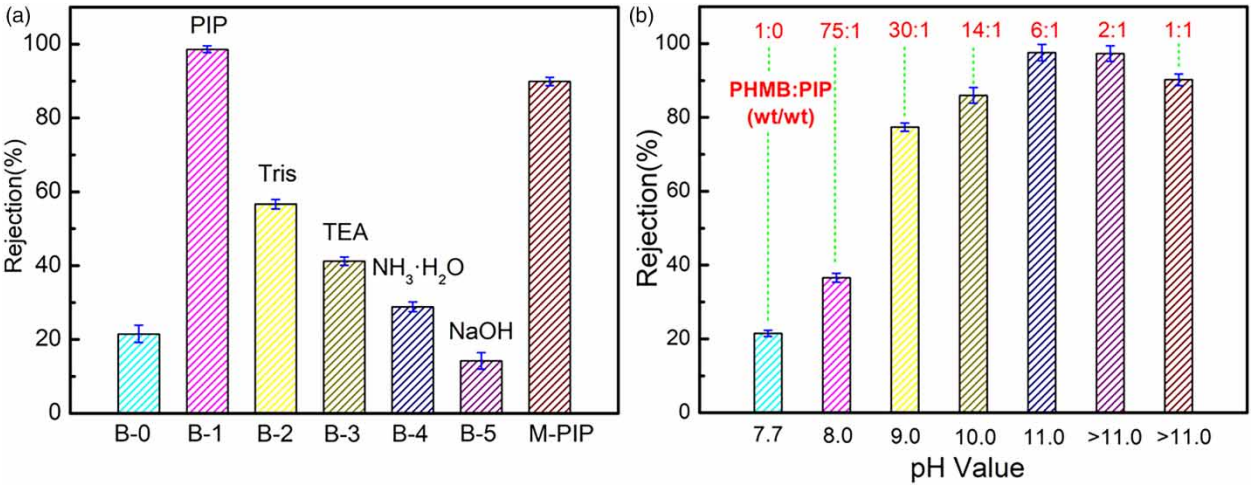

Figure 2 | Selection of aqueous base (a) and the relationship of PIP content to $MgCl_2$ rejection (1.0 g/L) of PHMB membranes (b).

increased, the rejection gradually decreased as high concentration of aqueous monomer did not match the 0.2% TMC concentration needed to prepare a compact network. Therefore, PIP was used as a regulator and the aqueous pH value was fixed at 11. According to the recipe of PHMB, pure $MgCl_2$ removal rate by PHMG–PIP membrane (**G-1**) was 97.3% while the value was 54.7 using pure PHMG membrane, supplementary table (Table S1).

3.2. Membrane structure characterization

Adjusted by PIP, both PHMB and PHMG membranes obtained ideal removal rates for $MgCl_2$. Thereafter, the structures of these two composite membranes were characterized and their performances were further investigated in water treatment applications. Surface chemistry of the membranes was analyzed by ATR-IR and XPS (Figure 3). Through ATR-IR spectra (Figure 3(a)), it was confirmed that there was a composite layer formed on the PSF support. The broad peaks at 3,400 cm^{-1} were -**N-H** stretching in **G-1**, **B-1** and **M-PIP** curves. The peak sizes were positively correlated with the numbers of -**N-H** groups. Guanidine-containing surfaces obviously possessed larger areas than M-PIPs. Peaks at 2,930^{-1} of **G-1** and **B-1** were -$\mathbf{CH_2}$- stretching in hexamethyl groups. The small peaks at 2,168 cm^{-1} were attributed to the terminal -**C ≡ N** group of PHMG and PHMB chains. The doublets at 1,623 cm^{-1} were -**C = O** stretching in amide groups, which indicated that polyamide layers were successfully prepared on PSF membranes. The order of peak sizes was **B-1** > **G-1** > **M-PIP**, which illustrated that there were more amide groups in guanidine membrane surfaces than for **M-PIP**s. In addition, **B-1** contained more amide bonds as biguanidine contained more -**N-H** groups than mono-guanidine. Therefore, the surface compactness was **B-1** > **G-1** > **M-PIP**. It was also confirmed by $MgCl_2$ filtration test.

Figure 3(b)–3(d) shows C1s high resolution of XPS curves of membrane surfaces. The insert in Figure 3(b) shows the element scanning spectra of membranes. Oxygen element contents in **G-1** and **B-1** were smaller than **M-PIP** due to the introduction of polyguanidine. Both **G-1** and **B-1** possessed peaks at 286.2 eV (Figure 3(c) and 3(d)), which were the terminal -**C ≡ N** group in polyguanidines (East *et al.* 1997). Peaks at 288 eV were -**C = O** bonds in the polyamide network. Their areas were in the order of **B-1** (69,086.8) > **G-1** (62,522.6) > **M-PIP** (57,992.3), which corresponded with ATR-IR data.

The hydrophilicity of membrane surface was evaluated by surface DWCA and zeta potential. Figure 4(a) shows that DWCAs of composite membrane were all smaller than for the PSF membrane. It illustrated that more hydrophilic skins were formed on the top of the supporting layer. The initial DWCAs of **G-1** and **B-1** were 63° and 55° but they declined to 20° with time with a slightly different developing trend. DWCAs of polyguanidine membranes were smaller than **M-PIP**s, which demonstrated that the introduction of polyguanidine provided higher hydrophilicity for the surfaces. Figure 4(b) shows that **B-1** and **G-1** displayed properties of positve-charged membranes. Biguanidine introduced more positive charges to the membrane surface. The isoelectric points of **B-1**, **G-1** and **M-PIP** were pH 8.86, 7.82 and 4.84, respectively. Polyguanidine, as polycations, introduced large amounts of NH groups to the membrane surface, which dissociated into $-NH_3^+$ or $-NH_2^+$ while the classic **M-PIP** was a negative charged membrane.

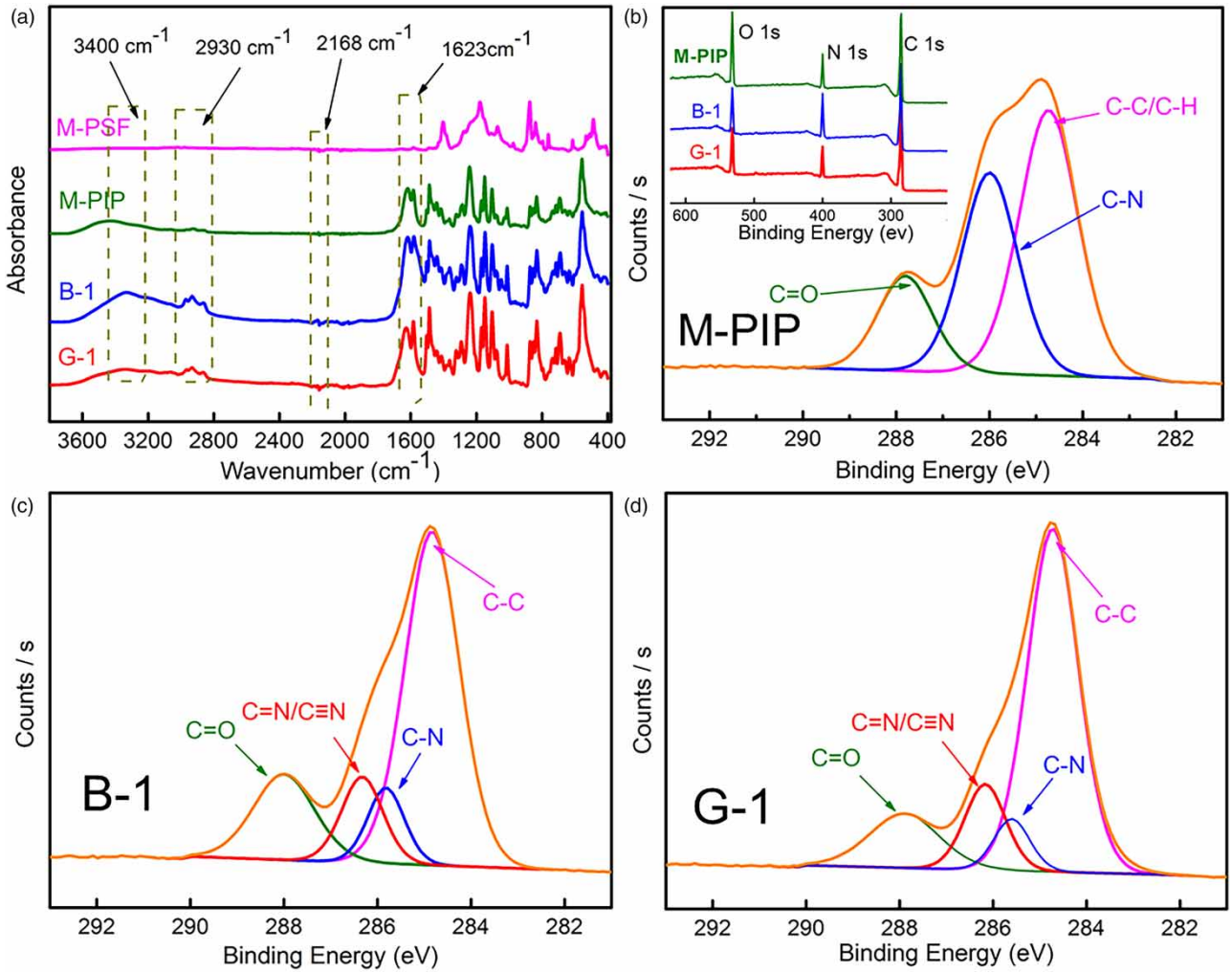

Figure 3 | ATR-IR and XPS spectra of membrane surfaces.

Micro-morphology of membranes was observed using FE-SEM and AFM (Figure 5). Through IP processes, PSF films were coated with composite layers. **G-1** and **B-1** did not have a typical nodular skin like the **M-PIP** membrane. There were irregular granular particles on the **G-1** surface, while B-1 had a very smooth skin. From cross-section images, the thicknesses of PA layers were 200, 200 and 160 nm for **M-PIP**, **B-1** and **G-1**, respectively. Surface roughness of composite membranes were higher than for PSF layers. The order of Ra values was **M-PIP** (12.00) > **G-1**(8.01) > **B-1**(6.93), which corresponded with the images observed by FE-SEM. Nodular size decreased as surface roughness and hence particles on **B-1** was the smallest. Polyguanidines were amphiphilic oligomers, which formed self-associated aggregates of 5 and 7 nm in aqueous phase, supplementary figure (Fig. S2). In these micelles, hydrophilic NH groups tended to distribute over the surface. This decreased migration speed from the aqueous phase to hexane during the IP process, which finally led to smoother surfaces (Li *et al.* 2014b; Jin *et al.* 2015). Biguanidine micelles possessed more hydrophilic surfaces as there were more NH groups in its structure.

3.3. Metal salts filtration performance

As positve-charged membranes, **B-1** and **G-1** displayed improved capacity for metal cations removal. In order to further investigate the membranes, filtration performances of **B-1** and **G-1** were evaluated through a series of metal salt filtration tests. Figure 6(a) provides water flux in filtration tests under 0.5 MPa. It can be seen that the PWF of **M-PIP** was lower than **B-1**'s and higher than **G-1**'s. **M-PIP** SWF of the $MgCl_2$ solution was 12.97 L m^{-2} h^{-1}. The SWF of the polyguanidine membranes were smaller than their PWF as there was osmotic pressure from the opposite direction to resist water permeating

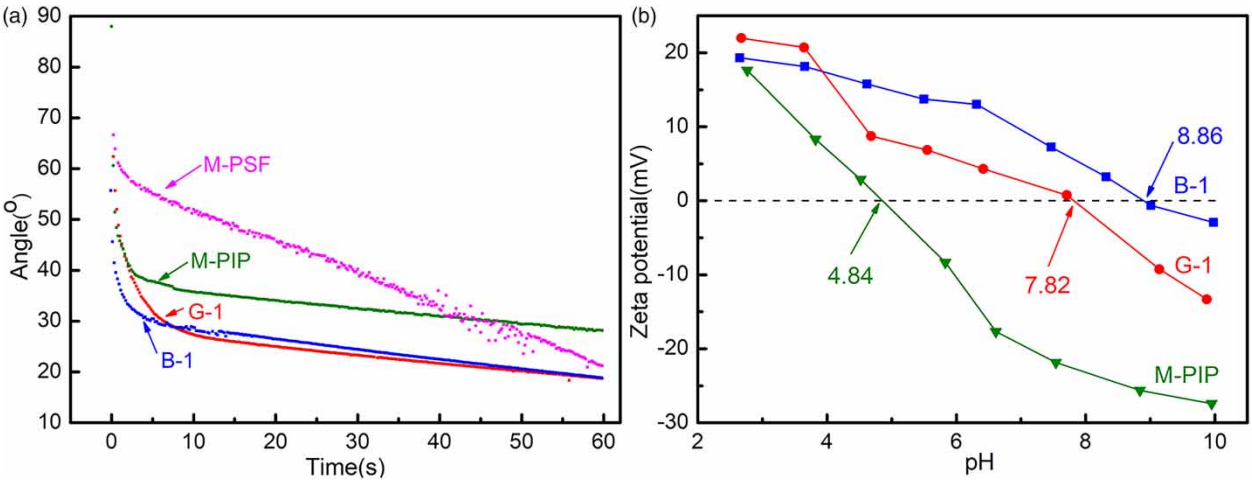

Figure 4 | DWCA (a) and zeta potential (b) of membrane surfaces.

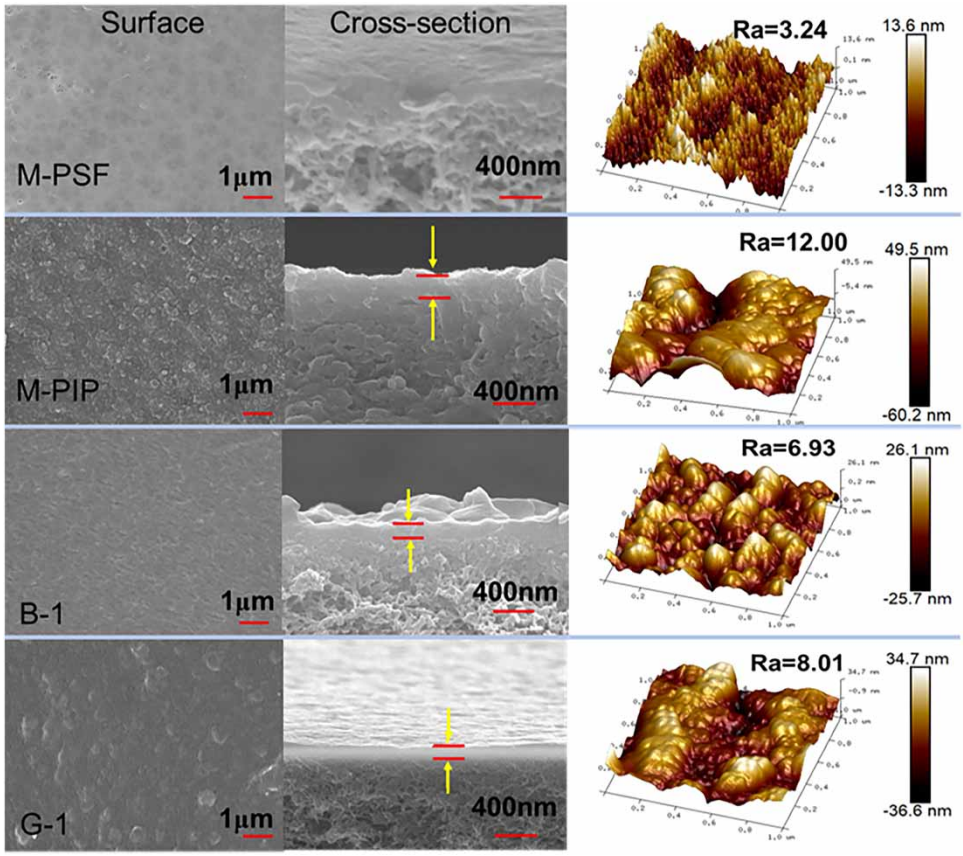

Figure 5 | FE-SEM and AFM images of membranes.

through the membrane. Either PWF or SWF of **B-1** was larger than **G-1**. This indicated that **B-1** had more cations on its surface, which provided a stronger repulsion to metal cations and led to the decrease in salt flux. Under a fixed pressure, the total flux of salt and water was fixed. As a result, the water flux of the salt solution increased although **B-1** had a more compact surface.

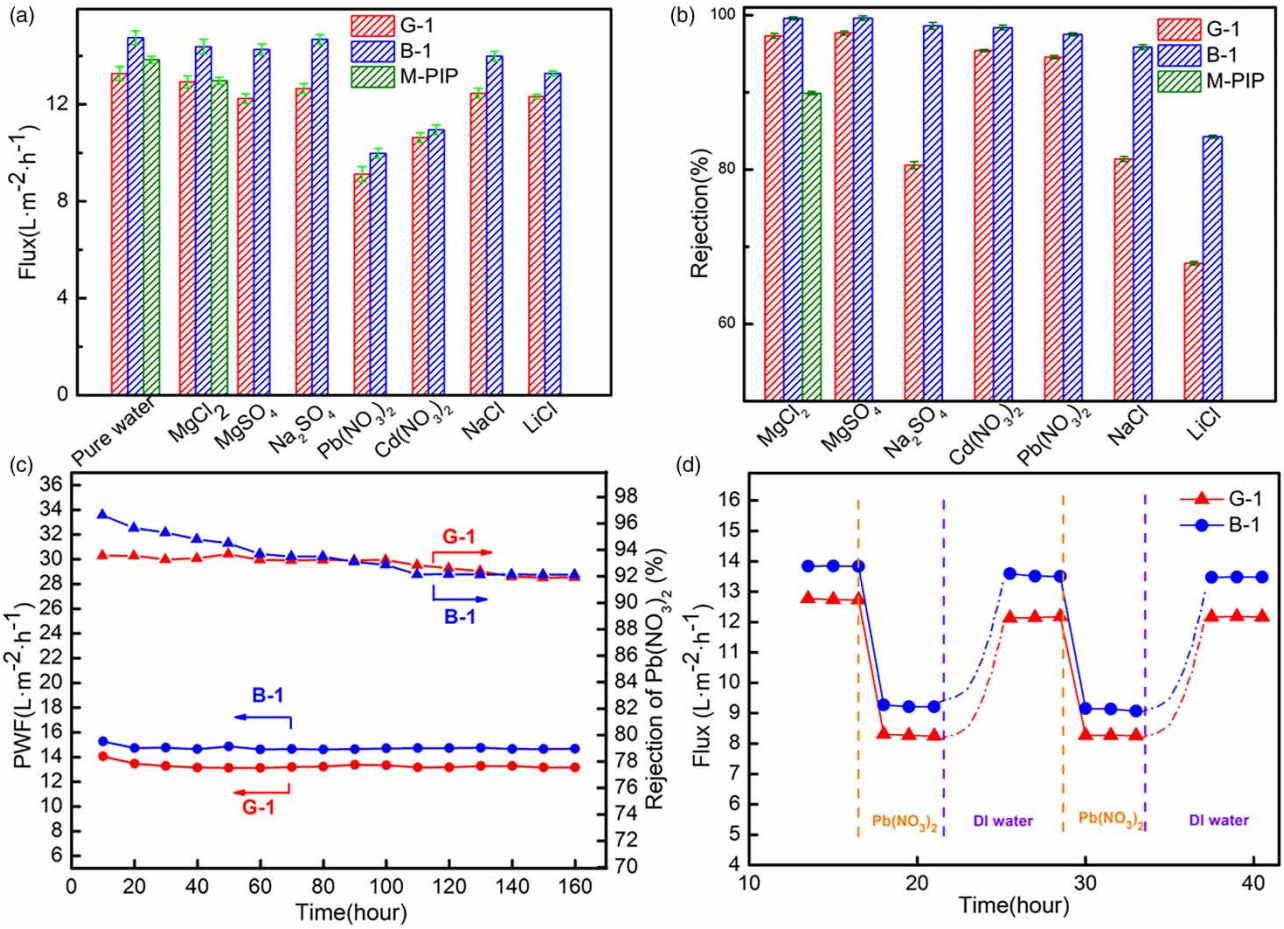

Figure 6 | Water flux (a) and retention (b) of membranes; long-term filtration of $Pb(NO_3)_2$ by **B-1** and **G-1** (c); and time-dependent FRR (d).

The salt rejections by **B-1** and **G-1** are shown in Figure 6(b). **B-1** displayed better salt removal performance than **G-1** in all salt filtration. Except for LiCl, the retention rates were higher than 95%. This could be attributed to more positive charges on **B-1** that provided greater repulsion to metal cations, especially multivalent cations. **G-1** provided larger retention differences between multivalent and monovalent cations. The rejection of **G-1** for divalent salts was all higher than 90%, while for sodium salts, Na_2SO_4 and NaCl, the values were 80.6% and 81.3%, respectively. The rejection of LiCl was only 67.0% as Li^+ was a monovalent cation and its hydration radius was comparatively small. The order of retention of **B-1** to salts was: $MgSO_4 > MgCl_2 > Na_2SO_4 > Cd(NO_3)_2 > Pb(NO_3)_2 > NaCl > LiCl$. The rejection order of **G-1** to salts was: $R(MgSO_4) > R(MgCl_2) > R(Cd(NO_3)_2) > R(Pb(NO_3)_2) > R(NaCl) > R(Na_2SO_4) > R(LiCl)$. It has been well known that classic **M-PIP** showed poor removal capacity for hazardous metal cations, such as Cd^{2+} and Pb^{2+}, because of their strong complex with the negative charged surface. However, the complex would be resisted to some degree if positive electrostatic repulsion from the membrane surface was strong enough. Thereafter, the membrane could obtain the capacity to remove hazardous heavy metal cations from polluted water. To prove this, filtration tests of a $1\ g{\cdot}L^{-1}$ $Pb(NO_3)_2$ solution by **B-1** and **G-1** were performed (Figure 6(c)). Water flux of both membranes faintly decreased from $14.9\ L{\cdot}m^{-2}{\cdot}h^{-1}$ to $14.4\ L{\cdot}m^{-2}{\cdot}h^{-1}$ for **B-1** and from $13.5\ L{\cdot}m^{-2}{\cdot}h^{-1}$ to $13.1\ L{\cdot}m^{-2}{\cdot}h^{-1}$ for **G-1** within a week. $Pb(NO_3)_2$ retention by **B-1** slightly decreased at the beginning and then remained above 92.1%. The interception of **G-1** decreased from 93.6% to 91.7%. The antifouling capacity of membranes was investigated through flux recovery tests of alternate $Pb(NO_3)_2$ filtration and water rinsing. FRR (Figure 6(d)) of **B-1** and **G-1** were 93.59% and 92.48%, respectively. XPS spectra showed that the chemistry of both membranes had not changed obviously after filtration of the $Pb(NO_3)_2$ solution, supplementary figure (Fig. S3). This confirmed that their surfaces were not polluted with heavy metal cations.

3.4. Separation of Li^+ and Mg^{2+}

From above, guanidine membranes exhibited discriminating removal rates for monovalent and multivalent metal cations. This property gave it the potential for enriching Li^+ from its mixed solution with Mg^{2+}, which is crucial in Li-ion battery resource preparation. Therefore, the Mg^{2+}/Li^+ separation was investigated through filtration of $MgCl_2$ and LiCl mixed solution. The solution concentration was 3.6 $g{\cdot}L^{-1}$ with the Mg^{2+}/Li^+ mass ratio as 60. After filtration, the mass ratios were 1.7 for **B-1** and 3.7 for **G-1**, respectively. The proportion of Li^+ in both permeations increased significantly (Table 1). Differently, both Mg^{2+} and Li^+ concentration decreased after filtration by **B-1**, but Li^+ content increased in the permeation of **G-1** according to negative rejection, which carried out the enrichment of Li^+. This could be explained by the solution-diffusion model (Li *et al.* 2021) as follows:

$$J_w = L_w(\Delta P - \sigma\Delta\pi) \tag{5}$$

where J_W was the water flux, L_W was the water permeation coefficient, ΔP was the operating pressure difference, σ was reflection coefficient and $\Delta\pi$ was the osmosis pressure:

$$J_s = P_s(\beta c_1 - c_2) \tag{6}$$

where J_S was the salt flux, P_S was the salt permeation coefficient, β was the polarization factor of the concentration difference, and c_1 and c_2 were the salt concentrations on the upstream and downstream sides of the membrane, respectively:

$$\beta = \frac{c_b}{c_m} \tag{7}$$

where c_b was the salt concentration on the membrane surface and c_m was the salt concentration of the bulk solution.

Owing to the large surface repulsion from the positive charge membrane, cation concentration over the surface area was lower than the bulk solution. Since Mg^{2+} suffered larger repulsion, the concentration over surface area ($c_{m,Mg^{2+}}$) should be smaller than for the bulk solution ($c_{b,Mg^{2+}}$). Comparably, Li^+ had low co-ion charge, which made it have smaller repulsion. It was easier for Li^+ to diffuse to the surface area to keep cation concentration homogeneity and charge equilibrium in the whole solution. As a result, c_{m,Li^+} (Li^+ concentration on the membrane surface) was higher than c_{b,Li^+} (Li^+ concentration in the bulk solution). Hence, the ratio of Mg^{2+} to Li^+ over the membrane surface was smaller than in the bulk solution. Furthermore, Li^+ had smaller hydrated radii than Mg^{2+}, which made it easier to be 'pushed' through the membrane to maintain electrostatic neutrality equilibrium under Donnan exclusion and steric hindrance mechanisms. More Li^+ permeating through the membrane resulted in a downstream concentration increase.

Long-time Mg^{2+}/Li^+ separation test was carried out to investigate the enrichment performance of Li^+ by **G-1** using 3.6 $g{\cdot}L^{-1}$ $MgCl_2$ and LiCl mixed solution and the result was graphed as shown in Figure 7. In 80 h, the rejection rate of Mg^{2+} and Li^+ decreased together to different degrees. Mg^{2+} retention slightly decreased from 92.4% to 83.7%, while Li^+ rejection declined from −3.6% to −21.5%. The separation factor of Mg^{2+}/Li^+ began to fall from 14.1 to 8.7 after 15 h and then remained steady.

3.5. Antimicrobial performance

PHMB and PHMG are mainly used as bactericides in preservatives or disinfectant. Therefore, the antimicrobial performance of **B-1** and **G-1** was investigated through colony formation experiments using Gram-negative E.C. and Gram-positive S.A bacteria as models. Figure 8 shows the digital photographs of dishes containing bacteria-inoculated agar. Both **B-1** and **G-1** exhibited excellent antibacterial capacities. Bactericidal rates of membranes were higher than 99% even though the culture

Table 1 | Results of Mg^{2+}/Li^+ separation

	$R_{mixture}$ (%)		Mg^{2+}: Li^+(w:w)		
Name	**Mg^{2+}**	**Li^+**	**Feed**	**Permeate**	**$S_{Li,Mg}$**
B-1	99.1	77.0	60:1	1.7:1	26.4
G-1	92.4	−3.6	60:1	3.7:1	14.1

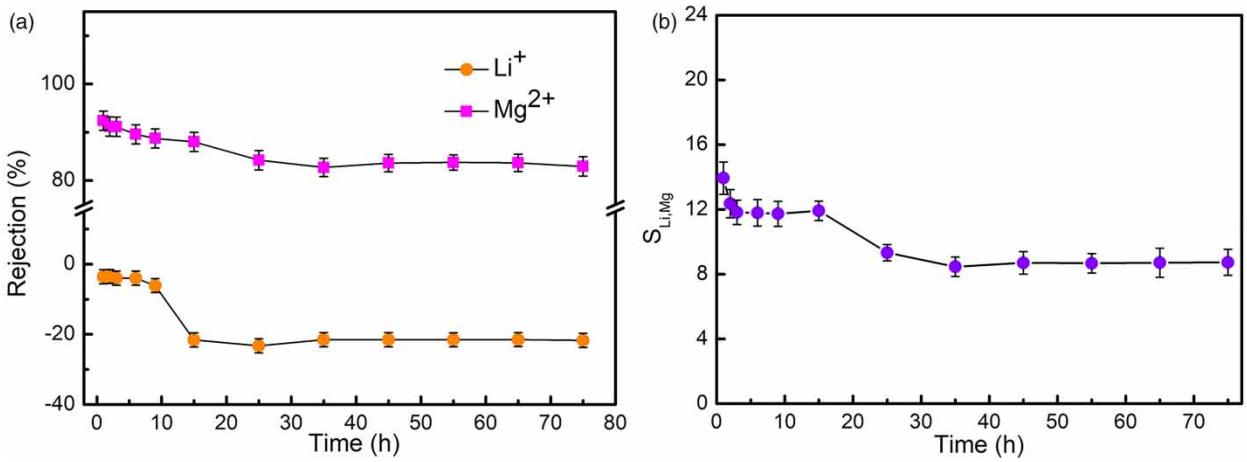

Figure 7 | Long-time Mg^{2+}/Li^{+} separation of **G-1**: Rejection (a) and separation factor (b).

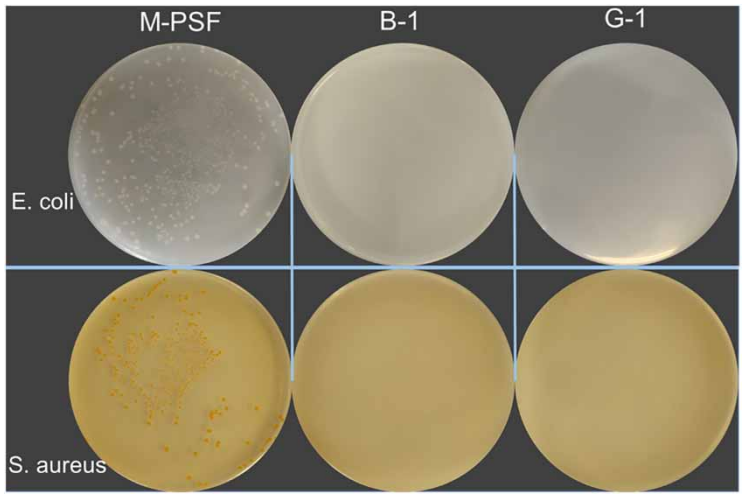

Figure 8 | Antibacterial results of membranes.

liquid had been diluted 1,000 times, supplementary figure (Fig. S4). SEM images showed that the cell walls of E. C. and S. A. were destroyed after contact with guanidine membranes, supplementary figure (Fig. S5). The result illustrated that polyguanidine chains still displayed excellent antibacterial ability even though they were fixed in a cross-linking network. Guanidine groups could dissociate into positive charges through partially forming amide groups, which ensured the biocide capacity. It was the polyguanidine micelle, that participated in the IP reaction but not single free molecules. There were still many unreacted NH groups left to dissociate into $-NH_3^+$ or $-NH_2^+$ to play a role in sterilization.

4. CONCLUSION

PHMB and PHMG are polycations. Under the assistance of PIP, they were successfully introduced onto the surfaces of the NF composite membrane through a IP reaction and prepared the positve-charged membranes. The membranes displayed excellent performance in multivalent metal salts removal from water. In particular, the long-time rejection of $Pb(NO_3)_2$ was higher than 90%, which provided the potential for hazardous heavy metal cation removal. Polyguanidine membranes showed moderate rejection of monovalent metal cations and retention of LiCl was only 67% by **G-1**. In the Mg^{2+}/Li^{+} mixture filtration, **G-1** decreases the Mg^{2+}/Li^{+} ratio from 60 to 3.7 accompanied with a negative Li^{+} rejection of −3.6. It exhibited the possible application in Li^{+} enrichment. In addition, both **B-1** and **G-1** showed excellent bactericidal performance in E.C. and S.A. tests as plenty of NH was left to dissociate into $-NH_3^+$ or $-NH_2^+$ after the IP process. Polyguanidine is a species of

promising oligomers in water treatment membrane preparation, including mono-/di-valent cation separation and hazardous heavy metal cation removal.

ACKNOWLEDGEMENT

The authors acknowledge the financial support from the National Natural Science Foundation of China (Grant Nos. 22075206, 21875162) and Tianjin Key Projects of New Materials Science and Technology (17ZXCLGX00050).

DATA AVAILABILITY STATEMENT

All relevant data are included in the paper or its Supplementary Information.

REFERENCES

Ahmad, N. N. R., Ang, W. L., Leo, C. P., Mohammad, A. W. & Hilal, N. 2021 Current advances in membrane technologies for saline wastewater treatment: a comprehensive review. *Desalination* **517**, 115170.

Akbari, A., Fakharshakeri, Z. & Rostami, S. M. M. 2016 A novel positively charged membrane based on polyamide thin-film composite made by cross-linking for nanofiltration. *Water Sci. Technol.* **73** (4), 776–789.

An, Q., Feng, L., Ji, Y. & Chen, H. 2011 Influence of polyvinyl alcohol on the surface morphology, separation and anti-fouling performance of the composite polyamide nanofiltration membranes. *J. Membr. Sci.* **367** (1–2), 158–165.

Bi, Q. Y., Zhang, C., Liu, J. D., Cheng, Q. & Xu, S. A. 2020 A nanofiltration membrane prepared by PDA-C_3N_4 for removal of divalent ions. *Water Sci. Technol.* **81** (2), 253–264.

Bi, Q. Y., Zhang, C., Liu, J. D., Liu, X. L. & Xu, S. A. 2021 Positively charged zwitterion-carbon nitride functionalized nanofiltration membranes with excellent separation performance of Mg^{2+}/Li^{+} and good antifouling properties. *Sep. Purif. Technol.* **257**, 117959.

Bodzek, M., Konieczny, K. & Kwiecinska-Mydlak, A. 2020 Application of nanotechnology and nanomaterials in water and wastewater treatment: membranes, photocatalysis and disinfection. *Desalin. Water Treat.* **186**, 88–106.

Chindera, K., Mahato, M., Sharma, A. K., Horsley, H., Kloc-Muniak, K., Kamaruzzaman, N. F., Kumar, S., McFarlane, A., Stach, J., Bentin, T. & Good, L. 2016 The antimicrobial polymer PHMB enters cells and selectively condenses bacterial chromosomes. *Sci. Rep-UK* **6**, 23121.

Domenech, N. G., Purcell-Milton, F. & Gun'ko, Y. K. 2020 Recent progress and future prospects in development of advanced materials for nanofiltration. *Mater. Today Commun.* **23**, 24.

East, G. C., McIntyre, J. E. & Shao, J. 1997 Polybiguanides: synthesis and characterization of polybiguanides containing hexamethylene groups. *Polymer* **38** (15), 3973–3984.

Fang, C. J., Sun, J., Zhang, B., Sun, Y. C., Zhu, L. P. & Matsuyama, H. 2018 Preparation of positively charged composite nanofiltration membranes by quaternization crosslinking for precise molecular and ionic separations. *J. Colloid Interface Sci.* **531**, 168–180.

Hou, A. Q., Zhou, M. E. & Wang, X. J. 2009 Preparation and characterization of durable antibacterial cellulose biomaterials modified with triazine derivatives. *Carbohydr. Polym.* **75** (2), 328–332.

Jin, J. B., Liu, D. Q., Zhang, D. D., Yin, Y. H., Zhao, X. Y. & Zhang, Y. F. 2015 Preparation of thin-film composite nanofiltration membranes with improved antifouling property and flux using 2,2′-oxybis-ethylamine. *Desalination* **355**, 141–146.

Li, X., Cao, Y. M., Yu, H. J., Kang, G. D., Jie, X. M., Liu, Z. N. & Yuan, Q. 2014a A novel composite nanofiltration membrane prepared with PHGH and TMC by interfacial polymerization. *J. Membr. Sci.* **466**, 82–91.

Li, Y., Su, Y., Dong, Y., Zhao, X. & Zhao, J. 2014b Separation performance of thin-film composite nanofiltration membrane through interfacial polymerization using different amine monomers. *Desalination* **333** (1), 59–65.

Li, S. L., Shan, X. Y., Zhao, Y. F. & Huo, Y. X. 2019 Fabrication of a novel nanofiltration membrane with enhanced performance via interfacial polymerization through the incorporation of a new zwitterionic diamine monomer. *ACS Appl. Mater. Interfaces* **11** (45), 42846–42855.

Li, N., Guo, C. S., Shi, H. T., Xu, Z. W., Xu, P., Teng, K. Y., Shan, M. J. & Qian, X. M. 2021 Analysis of Mg^{2+}/Li^{+} separation mechanism by charged nanofiltration membranes: visual simulation. *Nanotechnology* **32** (8), 085703.

Meng, J. Q., Zhang, X., Ni, L., Tang, Z., Zhang, Y. F., Zhang, Y. J. & Zhang, W. 2015 Antibacterial cellulose membrane via one-step covalent immobilization of ammonium/amine groups. *Desalination* **359**, 156–166.

Meng, M. J., Li, B. R., Zhu, Y., Yan, Y. S. & Feng, Y. H. 2021 A novel mixed matrix polysulfone membrane for enhanced ultrafiltration and photocatalytic self-cleaning performance. *J. Colloid Interface Sci.* **599**, 178–189.

Mohammad, A. W., Teow, Y. H., Ang, W. L., Chung, Y. T., Oatley-Radcliffe, D. L. & Hilal, N. 2015 Nanofiltration membranes review: recent advances and future prospects. *Desalination* **356**, 226–254.

Padaki, M., Isloor, A. M., Fernandes, J. & Prabhu, K. N. 2011 New polypropylene supported chitosan NF-membrane for desalination application. *Desalination* **280** (1–3), 419–423.

Qi, Y. W., Zhu, L. F., Shen, X., Sotto, A., Gao, C. J. & Shen, J. N. 2019 Polythyleneimine-modified original positve-charged nanofiltration membrane: removal of heavy metal ions and dyes. *Sep. Purif. Technol.* **222**, 117–124.

Sun, Y., Wang, Q., Wang, Y. H., Yun, R. P. & Xiang, X. 2021 Recent advances in magnesium/lithium separation and lithium extraction technologies from salt lake brine. *Sep. Purif. Technol.* **256**, 117807.

Wang, H. F., Zhang, Q. F. & Zhang, S. B. 2011 Positively charged nanofiltration membrane formed by interfacial polymerization of 3,3 ‘,5,5 ‘-biphenyl tetraacyl chloride and piperazine on a poly(acrylonitrile) (PAN) support. *J. Membr. Sci.* **378** (1–2), 243–249.

Wang, W. Y., Chiou, J. C., Yip, J., Yung, K. F. & Kan, C. W. 2020 Development of durable antibacterial textile fabrics for potential application in healthcare environment. *Coatings* **10** (6), 520.

Xu, P., Wang, W., Qian, X., Wang, H., Guo, C., Li, N., Xu, Z., Teng, K. & Wang, Z. 2019 Positive charged PEI-TMC composite nanofiltration membrane for separation of Li^{+} and Mg^{2+} from brine with high Mg^{2+}/Li^{+} ratio. *Desalination* **449**, 57–68.

Yu, H. J., Cao, Y. M., Kang, G. D., Liu, J. H., Li, M. & Yuan, Q. 2009 Enhancing antifouling property of polysulfone ultrafiltration membrane by grafting zwitterionic copolymer via UV-initiated polymerization. *J. Membr. Sci.* **342** (1–2), 6–13.

First received 7 January 2022; accepted in revised form 10 March 2022. Available online 22 March 2022